Novel Anatase TiO2 Boxes and Tree-like Structures Assembled by Hollow Tubes: D,L-Malic Acid-Assisted Hydrothermal Synthesis, Growth Mechanism, and Photocatalytic Properties

ARTICLE *in* CRYSTAL GROWTH & DESIGN · MARCH 2009

Impact Factor: 4.89 · DOI: 10.1021/cg8010597

5 AUTHORS, INCLUDING:

Bo Hu
University of Science and Technology of C…
24 PUBLICATIONS **1,289** CITATIONS
SEE PROFILE

Shu-Hong Yu
University of Science and Technology of C…
368 PUBLICATIONS **15,658** CITATIONS
SEE PROFILE

CRYSTAL GROWTH & DESIGN
2009
VOL. 9, NO. 3
1511–1518

Novel Anatase TiO_2 Boxes and Tree-like Structures Assembled by Hollow Tubes: D,L-Malic Acid-Assisted Hydrothermal Synthesis, Growth Mechanism, and Photocatalytic Properties

Shu-Juan Liu, Xiao-Xi Wu, Bo Hu, Jun-Yan Gong, and Shu-Hong Yu*

Division of Nanomaterials & Chemistry, Hefei National Laboratory for Physical Sciences at Microscale, the School of Chemistry & Materials, University of Science and Technology of China, Hefei 230026, P. R. China

Received September 21, 2008; Revised Manuscript Received November 28, 2008

ABSTRACT: Novel anatase TiO_2 hollow boxes and tree-like structures assembled by hollow tubes with a surface area as high as 241.89 m^2/g can be synthesized in large scale by a simple hydrothermal method. A distinctive growth mechanism taking advantage of the gaps and cracks in rectangular particulates with a composition of $(TiO_2)_2 \cdot C_4H_6O_5 \cdot 6H_2O$ as template has been proposed, which results in a particular structure with a double-layer wall and several inserted layers or separated rooms in the anatase TiO_2 hollow boxes. The effects of the reaction time, temperature, and molar ratio between D,L-malic acid and $TiCl_4$ on the formation of anatase TiO_2 have been investigated in detail. The results demonstrate that a larger molar ratio of D,L-malic acid and $TiCl_4$ benefits the formation of TiO_2 hollow boxes with larger aspect ratios. Anatase TiO_2 tree-like structures assembled by hollow tubes can be obtained when the molar ratio is kept at 5.4. Moreover, these distinctive structures show excellent photocatalytic properties, which would find potential applications in photocatalytic fields.

1. Introduction

Shape-controlled synthesis of nano- or micromaterials provides new opportunities in exploring unique chemical and physical properties. Hollow nanostructures have attracted tremendous interest as a special class of materials compared to other solid counterparts, owing to their higher specific surface area, lower density and better permeation, and widespread potential applications in chemical reactors, drug delivery, catalysis, sensors, lightweight materials, and various new application fields.[1] Hollow structures can be fabricated by the use of various removable templates, such as monodisperse silica, polystyrene (PS), or carbon spheres[2] with controllable sizes, as well as the soft ones of emulsion droplets, polymer/surfactant micelles, or even gas bubbles.[3] In addition, hollow interiors also can be obtained by localized Ostwald ripening[4] or differential diffusion (Kirkendall effect)[5] within metastable solid microspheres.

Nowadays, considerable efforts have been devoted to synthesize various nonspherical hollow structures, and some promising results have been obtained recently. Octahedral Cu_2O nanocages were synthesized via a catalytic solution route in one pot.[6] Highly symmetric 18-faceted polyhedral nanocages of Cu_7S_4 can be prepared by treating the cubic Cu_2O nanocrystals with thiourea at 90 °C.[7] Co_3O_4 nanoboxes were fabricated using preformed dispersed surfactant cubic particles as templates.[8] Xia et al. used the aqueous etchant based on $Fe(NO_3)_3$ or NH_4OH for the dealloying process of Au/Ag alloys to obtain nanocages with controllable wall thickness and porosity.[9] Furthermore, platinum-functionalized octahedral SiO_2 nanocages were synthesized conveniently using a quasi-template method by Archer et al.[10] PbTe nanoboxes have been synthesized by Wang et al. using a solvothermal technique.[11] Octahedral CdS microcages in large scale can be templated by in situ sacrificial template approach.[12] Zeng et al. obtained the hollow SnO_2 octahedra based on two-dimensional aggregation of nanocrystallites.[13] Lavayen et al. reported that urchin-like spheres assembled by hollow tubes of V_2O_5 formed through radial self-organized arrangement of lamina then followed by the rolling of the lamina into nanotubes in 2006.[14] Sea-urchin shaped carbon nanostructured materials with carbon nanotubes immobilized on hollow carbon spheres were obtained by Hyeon et al.[15] In addition, α-MnO_2 hollow urchins[16] and PEG-directed microspheres assemblies of hollow ZnO nanorods[17] have also been prepared in large scale recently. The hollow structures obtained from these methods are mostly spherical. Nevertheless, none of them have referred to using the cracks or gaps in a solid material as templates for the synthesis of hollow structures in a reaction.

As one important semiconductor, TiO_2 has received considerable attention in the fields of photocatalysis and photoelectric conversion owing to its exceptional optical and electronic properties, nontoxicity, low cost, and long-term stability against photocorrosion and chemical corrosion.[18] Considering the special relationship between the morphology and properties, a variety of structures of TiO_2 have been reported such as nanorods,[19] nanowires,[20] nanotubes,[21] hollow spheres,[22] and so on. Recently, the special anatase TiO_2 single crystals, which show a large percentage of reactive facets of {001}, have been obtained by using hydrofluoric acid as a morphology controlling agent.[23] However, such unique anatase TiO_2 hollow boxes with a double-layered wall and inserted layer and urchin-like flowers assembled by hollow tubes have not been reported so far. This distinctive structure of TiO_2 hollow boxes would have great benefits for the applications.

In this paper, we report a facile hydrothermal approach to produce novel TiO_2 microboxes and tree-like structures assembled by hollow cubes via the conversion from the box-like particulates with cracks and a composition of $(TiO_2)_2 \cdot C_4H_6O_5 \cdot 6H_2O$. The influences of the detailed reaction conditions on the formation of such distinctive structures, as well as their photocatalytic properties, have been investigated.

2. Experimental Section

Materials and Preparation. All chemicals are analytical grade and used as received without further purification. At first, transparent $TiCl_4$

* To whom correspondence should be addressed. Fax: +86 551 3603040. E-mail: shyu@ustc.edu.cn.

10.1021/cg8010597 CCC: $40.75
Published on Web 01/21/2009

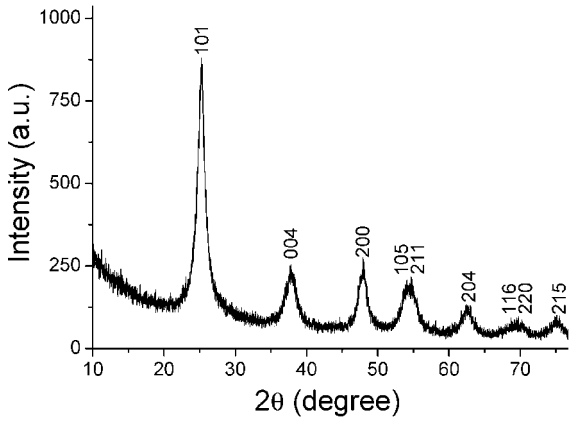

Figure 1. XRD pattern of the product prepared with R = 1:1 at 120 °C for 10 h.

solution was prepared by dripping 10 mL of $TiCl_4$ into 50 mL of deionized water, whose Ti^{4+} concentration was adjusted to 1.82 mol/L. In a typical procedure, 0.249 g of D,L-malic acid (about 1.82 mmol) and 0.3205 g of polyvinylpyrrolidone (PVP, the average molecular weight is about 40 000) was dissolved into 24 mL of deionized water and then 1 mL of $TiCl_4$ (1.82 mmol) solution was dropped into the solution above with continuous magnetic stirring. After this, the mixed solution was transferred into a 30 mL Teflon-lined autoclave and kept at 120 °C for 10 h. After being cooled down, the solution was filtered, washed by deionized water and absolute ethanol, respectively, and dried at 80 °C for several hours.

Photocatalytic Activity Measurement. One cyclindrical Pyrex flask with capacity of about 250 mL was used as the photoreactor vessel in the reaction system. About 50 mg of anatase TiO_2 boxes or Degussa P25 were put into the solution of acid fuchsine (100 mL) with a concentration of 100 mg/L as the catalyst. After being stirred in the dark for 15 min, then the whole reaction system was exposed to the light from a high pressure Xe lamp (150 W) from Perkin-Elmer Co. under stirring. Commercial TiO_2 (Degussa P25, Degussa Co.) was adopted as the reference to compare with the photocatalytic properties of the anatase TiO_2 prepared in the present study. UV−vis absorption spectra were recorded at different intervals to monitor the reaction.

Characterization. X-ray powder diffraction (XRD) patterns of the products were obtained on a Japan Rigaku DMax-γA rotation anode X-ray diffractometer equipped with graphite monochromatized Cu Kα radiation (λ = 1.54178 Å). Field emission scanning electron microscope (FESEM) images were taken on a field emission scanning electron microscope (JEOL JSM-6700F, 15 kV). Transmission electron microscope (TEM) photographs were taken on a Hitachi model H-800 transmission electron microscope at an accelerating voltage of 200 kV. High-resolution transmission electron microscope (HRTEM) photographs and selected area electron diffraction (SAED) patterns were performed on a JEOL JEM 2011 microscope at an accelerating voltage of 200 kV. X-ray fluorescence (XRF) was measured on an XRF-1800 X-ray fluorescence spectrometer (Shimadzu Corporation) at room temperature. UV−vis spectra were recorded on the Shimadzu UV-240 spectrophotometer at room temperature.

3. Results and Discussion

3.1. Controllable Synthesis of Anatase TiO_2 Boxes with Distinctive Structures. Figure 1 shows the X-ray diffraction (XRD) pattern of the as-prepared product obtained with a molar ratio of D,L-malic acid and $TiCl_4$ (R) as 1:1 at 120 °C for 10 h. As illustrated in Figure 1, all the diffraction peaks can be indexed as corresponding anatase TiO_2 phase with calculated cell parameters of a = 3.78 Å, c = 9.51 Å, which are in good agreement with those reported in the literature (JCPDS No. 83-2243). The diffraction peaks are much broadened, indicating the nanocrystalline nature of this sample.

FESEM images of the sample in Figure 2 show that more than 90% well-defined cuboid boxes of TiO_2 coexist with a small amount of irregular particles in the sample. Most boxes have a nearly rectangular bottom with each side about 2−3 μm and heights ranging from 7 to 9 μm. The magnified image in Figure 2B illustrates that walls of those boxes are composed of a large amount of tiny nanoparticles, despite the relative smooth surfaces. The inner structures of the boxes have been revealed by the broken ones (Figure 2C,D). The hollow boxes have double-layer walls, and some inserted layer or separate rooms may exist in the inside of the boxes. TEM images in Figure 3 revealed that mainly three kinds of inner structures are obtained in the TiO_2 boxes, that is, unclosed inserted layers, separate rooms closed with inserted layers, and hollow structures with nothing inside. The wall thickness of the box is relatively uniform and the value is about 100 nm. A typical HRTEM image (Figure 4B) taken from the framed part of the TiO_2 box (Figure 4A) indicates that the boxes are composed of a large number of tiny particles. The inserted electron diffraction pattern (ED) image in Figure 4A proves its polycrystalline nature further. The fringe spacing of 3.55 Å corresponds well to that of the (101) faces for anatase TiO_2.

3.1.1. Effect of Reaction Time. To understand the formation mechanism of such distinctive boxes, the detailed growth process of this product was carefully followed by time-dependent experiments. Analyzed from a series of XRD patterns with reaction times as shown in Figure 5, it can be concluded that the product initially formed in the reaction systems is not anatase TiO_2 but actually a precursor. It has been known that malic acid reacting with $TiCl_4$ could produce $(TiO_2)_2 \cdot C_4H_6O_5 \cdot 6H_2O$ crystals immediately,[24] which is confirmed by the X-ray fluorescence (XRF) analysis listed in Table 1. The atomic ratio of C:Ti is 1.87, which approximates the value of 2 in the above molecule. As reaction proceeds, a process of the further perfection of the crystallinity of the precursor, gradual decomposition of the precursor, emergence of the anatase TiO_2 nanoparticles, and finally the pure phase of anatase TiO_2 boxes is observed.

A series of FESEM and TEM images of the samples in Figure 6 show the morphology of the particles prepared at different reaction stages, reflecting the morphology transformation process of the precursor into anatase TiO_2 clearly. The immediate precipitates and the sample prepared after reaction for 1.5 h are cracked cuboids. TEM image in Figure 6B indicated that the particles are fragile at this stage. Besides, it seems that the cracks take place toward different directions (Figure 6D). From this, we could suppose rationally that the depth of the cracks should also vary significantly. As reaction proceeds to 5 h, the morphology of box and some aggregated particles come into being simultaneously. The corresponding TEM image in Figure 6F indicates that the cavitating process takes place in the reaction system at this stage. While further extending the reaction time to 8 h, only parts of particles are hollow, indicating the incomplete decomposition of the precursor further. As reaction time is increased to 8 h, more irregular particles will form (Figure 6G), which could be due to the nucleation and supersaturation occurring in bulk solution.

3.1.2. Effect of Temperature. The particles obtained at 100 °C are solid cuboids (Figure 7A,B) and the XRD pattern (Supporting Information, Figure S1A) reveals its essence of precursor. Although anatase TiO_2 is obtained at 140 °C, a large amount of particles and fragments coexist with a small quantity of intact boxes (Figure 7C and Supporting Information Figure S1B). It is well-known that a higher reaction temperature would often accelerate the reaction velocity; thus, the higher decomposition rate of the precursor would occur in the present system.

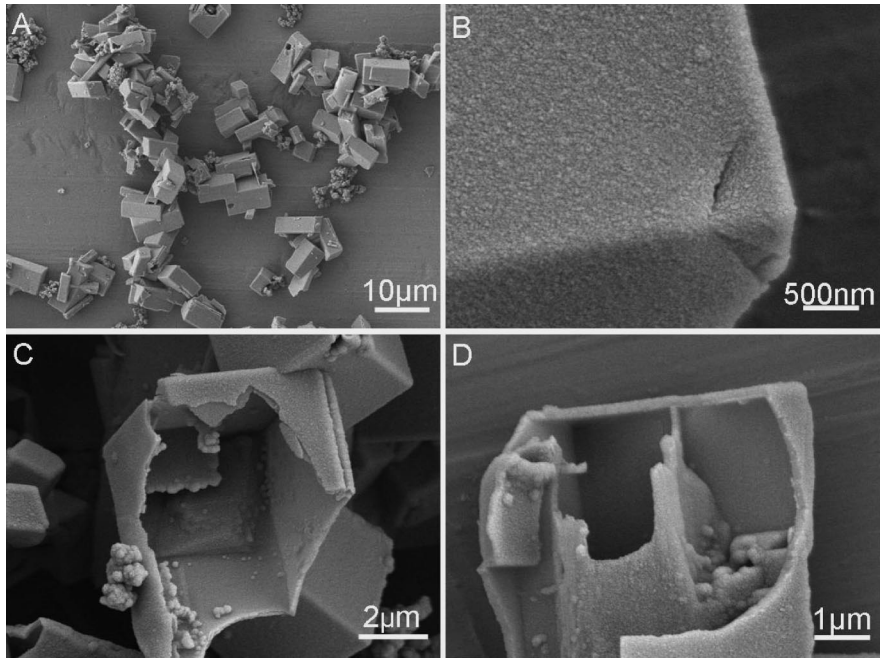

Figure 2. (A−D) FESEM images of the sample prepared at 120 °C for 10 h with R = 1:1.

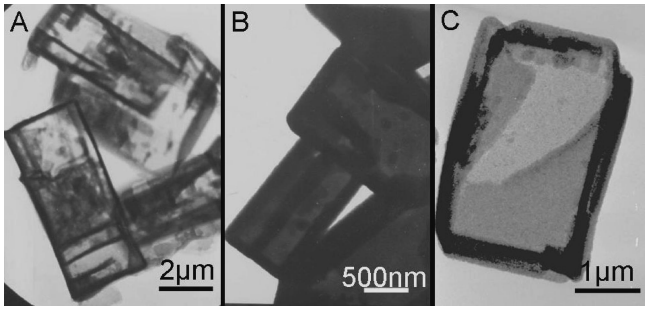

Figure 3. (A−C) TEM images of the sample obtained at 120 °C for 10 h with R = 1:1.

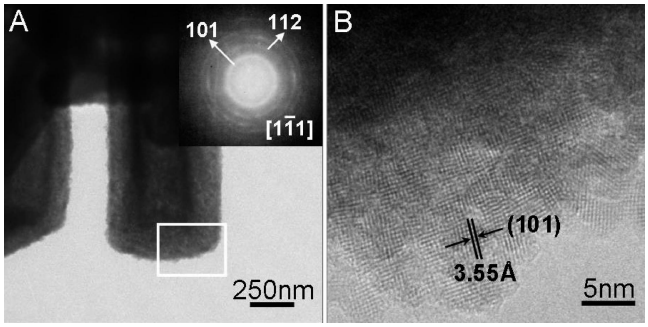

Figure 4. (A, B) HRTEM image and the corresponding ED pattern of the sample obtained at 120 °C for 10 h with R = 1:1.

Then, a large amount of anatase TiO_2 crystal nucleus resulting from the high reaction temperature would not have enough time to adhere onto the surfaces or the cracks of the precursor in bulk solution, leading to the formation of irregular particles which are not templated on the solid cuboids. All the above analyses indicate that a proper reaction temperature should have a great influence on the formation of a large number of intact antase TiO_2 boxes.

3.1.3. Effect of the Molar Ratio of D,L-Malic Acid and $TiCl_4$. In the present reaction system, the molar ratio of D,L-malic acid and $TiCl_4$ plays a significant role in the formation of hollow boxes with different morphologies and aspect ratios. At a low molar ratio of D,L-malic acid and $TiCl_4$, that is, R = 1:2, the aspect ratio of boxes decreases a little and the hollow structures with approximate cubic shapes are obtained. Although the uniformity of the particle sizes is not good, most boxes have edges with sizes of about 3.5 μm (Figure 8A,B). When the ratio increases to 1:1 as before, the length of those boxes have grown into 7 to 9 μm and the aspect ratio is about 3 or less (Figure 2). The product obtained at the ratio 2:1 is a mixture of a small quantity of tree-like structures and a relatively large amount of boxes with larger aspect ratios. Further increasing that to 5.4,

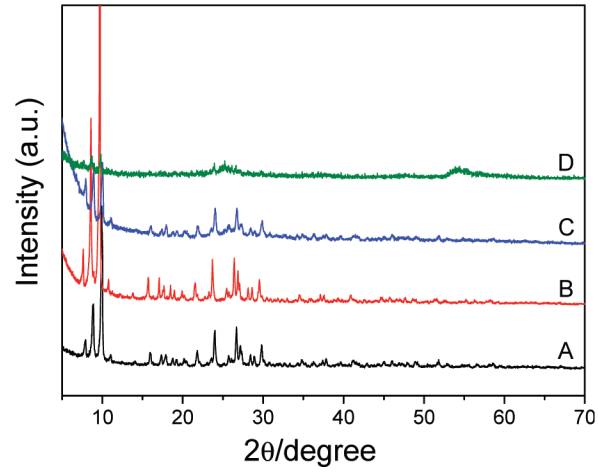

Figure 5. XRD patterns of the products prepared at 120 °C for different reaction times with R = 1:1. (A) Immediate precipitation from the solution at room temperature, (B) 1.5 h, (C) 5 h, and (D) 8 h.

Table 1. XRF Data of the Precursor

elements	weight %	atomic %
Ti	68.1064	34.89
C	31.8759	65.10
others	0.0177	0.01
total	100	100

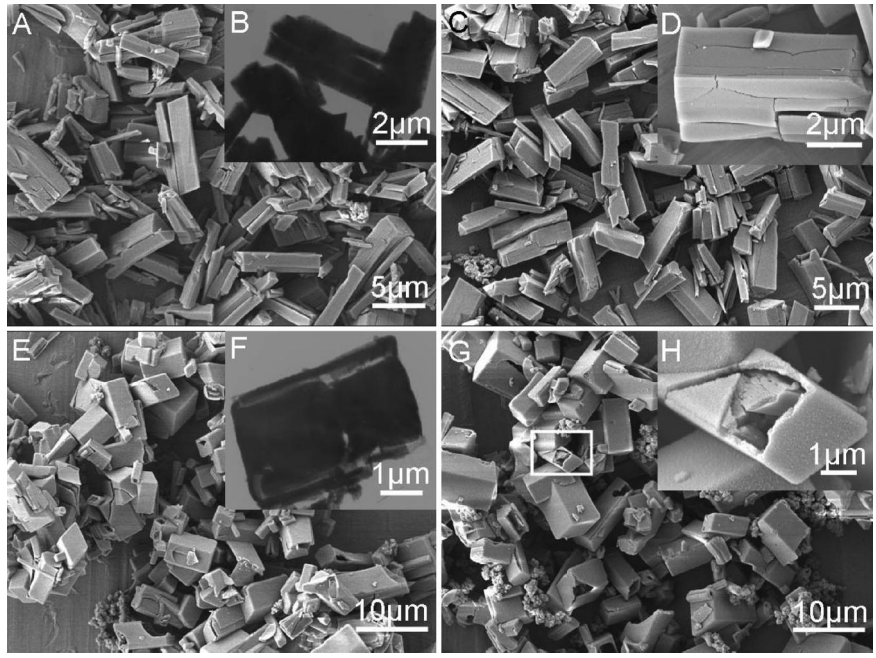

Figure 6. FESEM and TEM images of the samples prepared at 120 °C for different reaction times with R = 1:1 (A and B) the particles obtained after immediate precipitation. (C) and (D) 1.5 h, (E) and (F) 5 h, (G) and (H) 8 h.

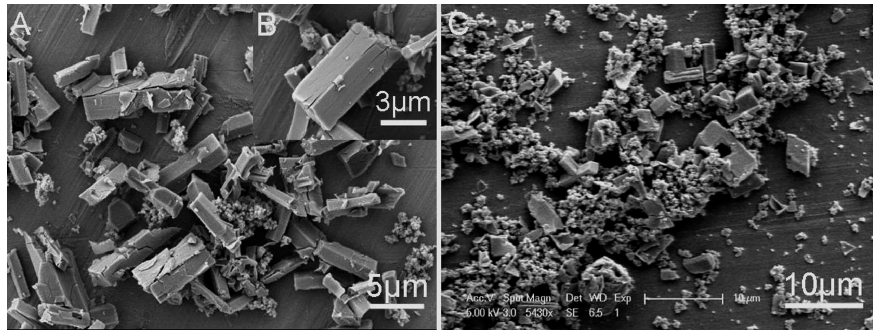

Figure 7. FESEM images of the samples prepared with R = 1:1 for 10 h at different reaction temperatures: (A) and (B) 100 °C, (C) 140 °C.

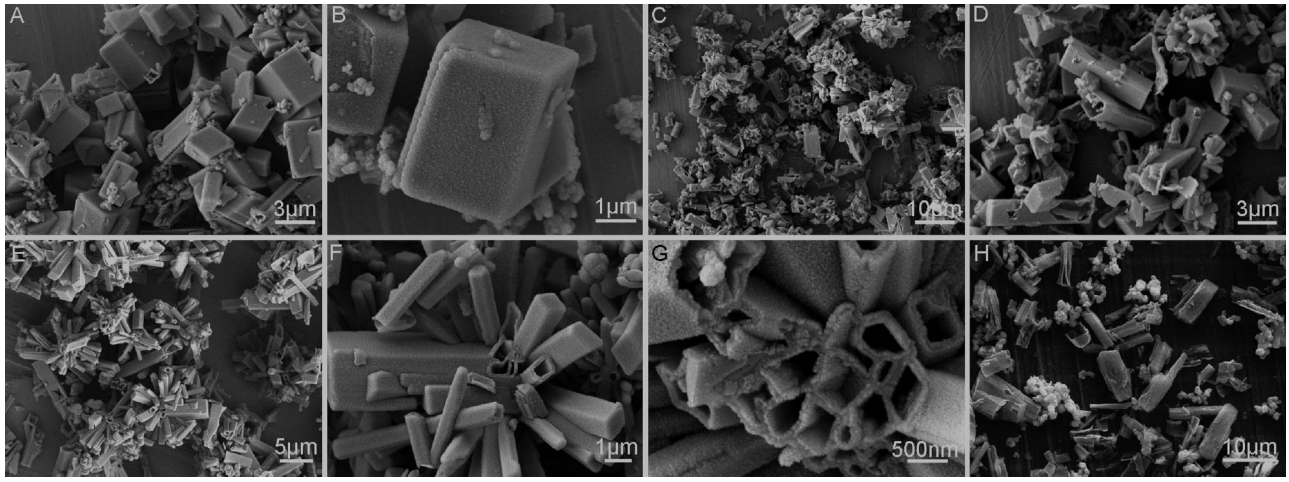

Figure 8. FESEM images of the samples obtained at 120 °C for 10 h with different molar ratios of D,L-malic acid and $TiCl_4$ (R). (A) and (B) R = 1:2, (C) and (D) R = 2:1; (E), (F) and (G) R = 5.4:1, and (H) R = 10:1.

it is interesting to find that a majority of tree-like structures assembled by thin hollow tubes on the main body of one big box are obtained (Figure 8E). As illustrated in Figure 8F, each closed tube in the superstructure grows with the root in the main big box and has the morphology of cuboids. Simultaneously, double-layer structure of the wall could be observed obviously in the Figure 8G and the thickness of every layer is about 60 nm. The total width of the roots in one flower is about 2.5 μm

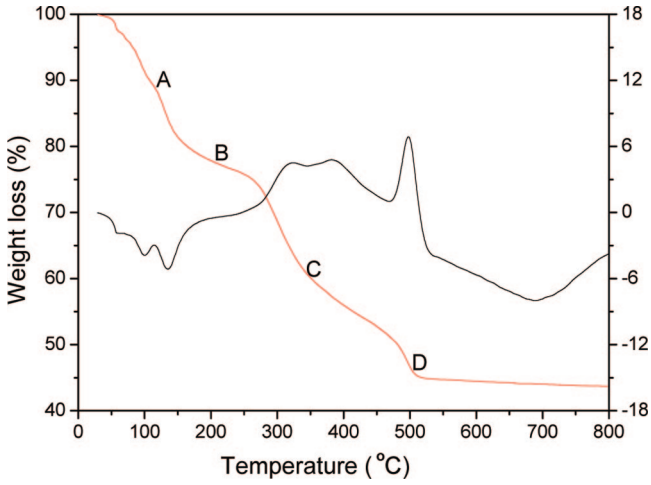

Figure 9. TG−DTA curves of the precursor obtained at 120 °C for 1.5 h with R = 1:1 in the presence of 0.3205 g of PVP.

or more, which corresponds well to the width of one box. As the amount of D,L-malic acid increases further until the molar ratio reaches 10:1, it is found that a large amount of irregular particles coexist with those boxes with larger aspect ratios in the system (Figure 8H).

Moreover, the effect of the PVP added in the reaction system was also examined. It is found that its addition is not absolutely essential for the formation of the hollow boxes, while the dispersibility of the hollow boxes could be influenced greatly. Without PVP in the reaction system, the hollow boxes would congregate together (Supporting Information, Figure S2). Thus, a proper amount of PVP would play a role as a dispersant in the reaction system.

3.2. Thermogravimetric Analysis of the Precursor $(TiO_2)_2 \cdot C_4H_6O_5 \cdot 6H_2O$. Thermogravimetric analysis (TGA) in Figure 9 shows that the precursor $(TiO_2)_2 \cdot C_4H_6O_5 \cdot 6H_2O$ in the atmosphere undergoes four steps during decomposition, that is, with a distinctive net weight loss of step A 10.1 wt % (up to 108 °C), step B 13.6 wt % (from 108 to 239 °C), step C 23.5 wt % (from 239 to 450 °C), and step D 9.0 wt % (from 450 to 750 °C). In contrast with the sample obtained without addition of PVP, the TG-DTA curves here show similar features (Supporting Information, Figure S3). Thus, it is rational to suppose that the decomposition process here has no relationship with the PVP and the PVP has been removed completely. Here, the steps A and B took place due to the loss of water; while other two steps went along with the decomposition of the precursor, anatase TiO_2 formed at last. It should be noted that the complete decomposition temperature of the precursor needs to be higher than 500 °C.

3.3. BET Analysis of the Anatase TiO_2 Hollow Boxes. The Brunauer−Emmett−Teller (BET) surface area of the hollow boxes was determined by N_2 adsorption using an ASAP-2020 surface area analyzer. The result shows that a large BET surface area of 241.89 m^2/g is obtained finally and most are taken by the external surface area, whose value is about 212.51 m^2/g. The N_2 adsorption−desorption isotherm and the pore size distribution curves of the anatase TiO_2 hollow boxes are illustrated in Figure 10. The hysteresis of the desorption branch (Figure 10A) is due to the hindered desorption which is often observed in the particulate samples.[25] While further observation indicates an abrupt change exists in this desorption branch, which may result from an abrupt change of the pores structure. As we have observed above, a large number of nanoparticles have constituted the wall of the boxes, and the pore size among

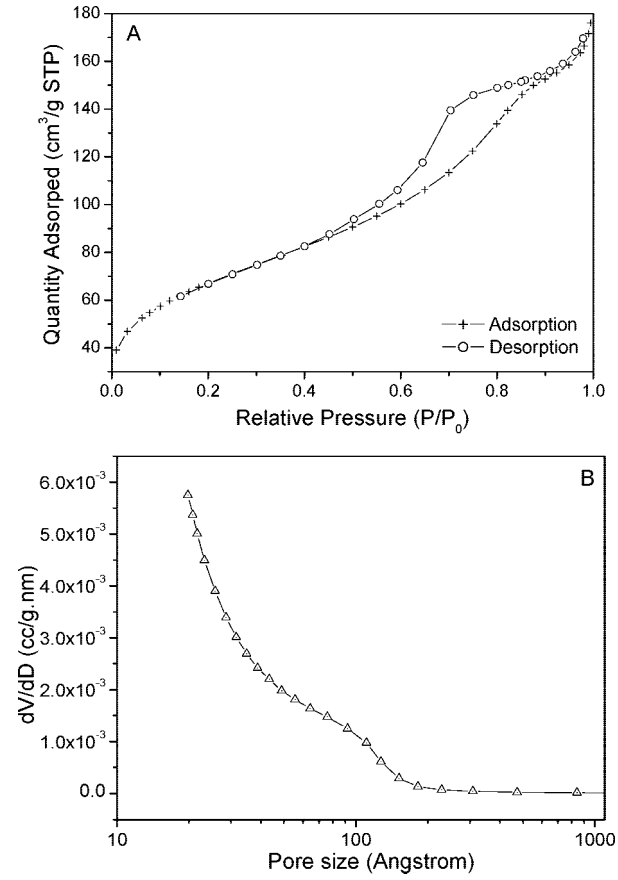

Figure 10. (A) N_2 adsorption−desorption isotherm curve and (B) pore size distribution of the sample obtained at 120 °C for 10 h with R = 1:1.

them is very small. However, the thickness of the layer clearance between the double layers of the walls of TiO_2 boxes is much larger than this pore size. When desorption takes place, just this abrupt change of the pore size in the structures will cause a distinctive desorption feature (Figure 10A). The broad distribution of pore size in the TiO_2 boxes has been proved further as shown in Figure 10B.

3.4. Reaction Mechanism. On the basis of the series of above analyses, a peculiar gap−template synthesis mechanism which has not been mentioned previously has been proposed to explain this phenomenon rationally. The reaction process could be described by two chemical reactions as follows:

$$2TiCl_4 + C_4H_6O_5 + 10H_2O \rightrightarrows (TiO_2)_2 \cdot C_4H_6O_5 \cdot 6H_2O + 8HCl \quad (1)$$

$$(TiO_2)_2 \cdot C_4H_6O_5 \cdot 6H_2O \rightrightarrows 2TiO_2 + C_4H_6O_5 + 6H_2O \quad (2)$$

To prove this assumption, the control experiment has been performed, in which the precursor obtained for 1.5 h is treated without HCl at 120 °C for another 8.5 h (Supporting Information, Figure S4). It is found that anatase TiO_2 boxes could also be formed. Thus, it is rational to propose that the formation of anatase TiO_2 boxes in the reaction system is just due to the decomposition of the precursor. Although much higher decomposition temperature was applied (Figure 9), the formation of anatase TiO_2 boxes under hydrothermal conditions should have a big difference from the decomposition process in the thermal analysis.[26]

The formation process of the distinctive anatase TiO_2 boxes has been illustrated in particular in Scheme 1. Large amounts

Scheme 1. Illustration of the Formation Process of the TiO_2 Hollow Boxes

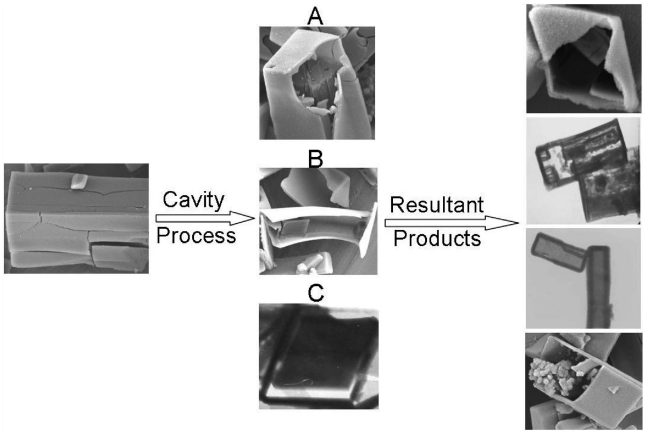

of white precursor of $(TiO_2)_2 \cdot C_4H_6O_5 \cdot 6H_2O$ is precipitated immediately after addition of $TiCl_4$ into the solution of D,L-malic acid, which may be due to its larger K_{sp} value. When the process of fast precipitation initially is over, then slow growth speed would take the dominant place in the whole reaction system. As the reaction proceeds, the solid structure of precursor whose inner has poor crystalline quality, while a better crystalline layer on the surface would form in the system.

As shown in the left image in Scheme 1, the fragile essence of this precursor has been revealed obviously and the surfaces are full of considerable cracks with different depths to different directions. From the theory of Ostwald ripening as occurred in other reaction systems, it is well-known that crystalline nanoparticles formed initially would often show higher surface energy and be not stable, which would have the greater tendency to dissolve or decompose.[4] Then, further prolonging the reaction time it could be found that the reaction (eq 2) will be a dominant reaction in the system, whose occurrence would shift the reaction to the second stage, that is, the formation of TiO_2 nanoparticles and emergence of cavitating process. As reaction proceeds further, it would be rational to suppose that the peculiar structure of the precursors would play a significant role as sacrificial templates in the subsequent reaction. On the assumption that we have made, the TiO_2 nanoparticles begin to precipitate on the surfaces and also in the various cracks of the precursor. Considering the better stability of the precursor surfaces when the reaction proceeds into the stage as illustrated in the middle part in Scheme 1, such as the one shown in image C, then the anatase TiO_2 nanoparticles would precipitate on the thin shell of the box both from the inner and the outside. Because of the presence of stable layer of precursor, which is coated by anatase TiO_2 nanoparticles from inner to outside, so when the reaction time is long enough that all the precursor are transformed into anatase TiO_2 then hollow boxes with double-layer walls will form finally. Furthermore, each crack has two surfaces with nearer distance to each other. The precipitation of the TiO_2 nanoparticles on the cracks is essentially a precipitation process on two surfaces. When the two precipitation layers approach so near that the attraction effect of van der Waals forces take the dominant place, then an inserted wall with double-layers would come into being. When several cracks intersect in the inner part or one crack could run through the precursor, then separate rooms with double-layer walls in the whole box would be observed frequently. The more these two kinds of cracks, the more separate rooms in the hollow boxes. When the cracks have been full of anatase TiO_2 nanoparticles, the nanoparticles formed afterward will precipitate on the surfaces of the boxes and the positions of the cracks. Thus, the cracks existing in the early precursor would disappear from the surfaces of the TiO_2 microboxes.

In addition, the existence of cracks in the cuboids also benefits the acceleration of the decomposition of precursors in the initial stage, and it should be another probable reason for the formation of the complex TiO_2 boxes with inserted layers or separate rooms. However, if an intact cuboid, in which no cracks could be found, is formed in the reaction system, then that kind of hollow box without any inserted layer could be obtained finally. Moreover, it needs to be noted that about 10% nanoparticles could be found in the resultant products. The careful observation in the initial precursor shows that also some small broken ones with irregular morphologies were observed besides most relatively regular cuboids in the system. Considering that the imperfect cracks may exist in the inner and exterior parts of the precursor particulates, it is not surprising at all that we could find nanoparticles both in the boxes and out of the boxes. In addition, due to the higher reaction velocity, a local supersaturation may exist in the bulk solution, which could allow the nucleation to take place away from the precursor template. This should be another rational reason for the formation of the irregular particles in the reaction system.

3.5. Photocatalytic Properties of the Anatase TiO_2 Hollow Boxes. To investigate the potential photocatalytic properties of these novel TiO_2 structures, a series of photocatalytic experiments were carried out in comparison with that of Degussa P25 under the exposure of UV light. Figure 11a shows the absorption spectra of the acid fuchsine solution catalyzed by anatase TiO_2 hollow boxes obtained at different molar ratios and the Degussa P25. The framed part in Figure 11A is shown clearly by the enlarged curves on the right (Figure 11B), indicating that the sample obtained with a molar ratio of 1:1 has the most outstanding photocatalytic properties among a series of anatase TiO_2 boxes. It is well-known that a proper amount of adsorbents on the surfaces of TiO_2 nanocrystals would have benefits for the separation of the hole and electron in the photocatalytic process. Then, the photocatalytic efficiency would be improved to some extent. When the amount of adsorbents coated on the surfaces is so large that it has influenced the adsorption of acid fuchsine then the TiO_2 would have worse photocatalytic properties. Considering the formation mechanism of TiO_2 hollow boxes and the possible adsorption of D,L-malic acid in the process, it is reasonable to believe that a higher molar ratio of D,L-malic acid and $TiCl_4$ will have worse photocatalytic properties for the TiO_2 boxes. In despite of a slight difference, the photocatalytic property of the one obtained at 1:1 approximates that of Degussa P25. To study the photodegradation process of the catalyst produced at 1:1, time-dependent experiments were performed with the absorption change of the acid fuchsine solution. From Figure 12, it could be concluded that after 45 min the peak at 545 nm has disappeared completely, which means the complete photodegradation of the acid fuchsine solution. The inset photograph in Figure 12 has reflected the color transformation process of the acid fuchsine solution with the photocatalytic degradation of the TiO_2 boxes. In addition, to prove the effect of the TiO_2 boxes for the acid fuchsine solution further, we have also conducted an experiment in which only acid fuchsine solution is exposed under the UV illumination without any catalyst. Indeed, the presence of TiO_2 boxes has played an indispensable role in the complete degradation of the acid fuchsine (Supporting Information,Figure S5). Considering the distinctive relationship between the morphology and properties, it would be rational to suppose that our synthesized novel

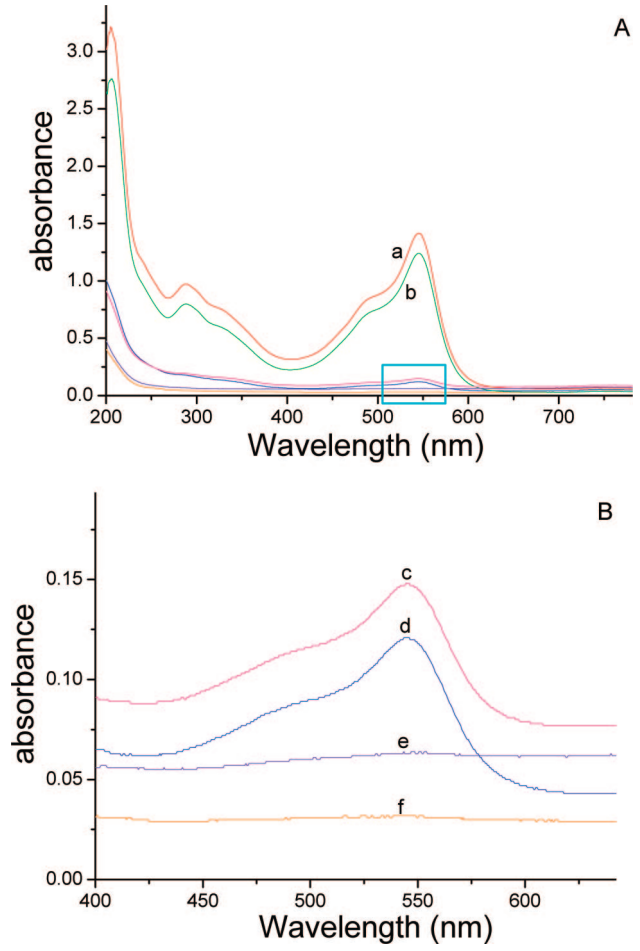

Figure 11. (A) Absorption spectra of the acid fuchsine solution catalyzed for 45 min by TiO_2 obtained at different molar ratios of D,L-malic acid and $TiCl_4$ and (B) is the enlarged part framed in (A): (a) 10:1, (b) 5.4:1, (c) 1:2, (d) 2:1, (e) 1:1, (f) P25.

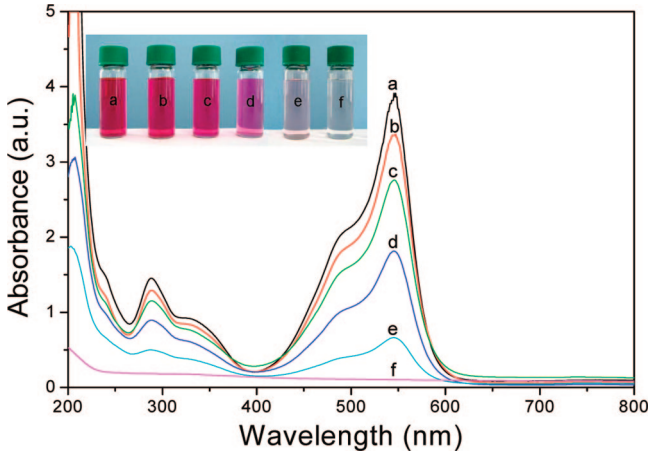

Figure 12. The absorption spectra of the acid fuchsine solution under exposure of the UV for different reaction times: (a) 0 min; (b) 5 min; (c)15 min; (d) 25 min; (e) 35 min; (f) 45 min.

structures of anatase TiO_2 would find potential applications as a photocatalyst.

4. Conclusions

In summary, novel anatase TiO_2 hollow boxes and tree-like structures assembled by hollow tubes have been synthesized under mild conditions by taking advantage of gaps/cracks on original precursor particulates as templates. It is demonstrated that the boxes grow with double-layer walls and there exist inserted layers or several separate rooms in the inner part. The influence of the reaction time, temperature, and molar ratio between D,L-malic acid and $TiCl_4$ on the formation of this distinctive structure have been investigated in detail. The precursor of $(TiO_2)_2 \cdot C_4H_6O_5 \cdot 6H_2O$ particulates with a lot of cracks is obtained initially and acts as the sacrificial template for the formation of TiO_2 hollow boxes. When the molar ratio of D,L-malic acid and $TiCl_4$ is kept at 5.4, the particular tree-like structures constructed by hollow tubes can be produced in a large scale. Moreover, the anatase TiO_2 obtained with a molar ratio of 1:1 have exhibited best photocatalytic properties, which would find potential applications as a photocatalyst. The present synthesis of the TiO_2 structures by using gaps or cracks as templates may provide a distinctive view and idea for the synthesis of other functional hollow inorganic structures.

Acknowledgment. S.H.Y. acknowledges the special funding support from the National Natural Science Foundation of China (NSFC, Grant Nos. 50732006, 20621061, 20671085, 20701035), 2005CB623601, the Specialized Research Fund for the Doctoral Program (SRFDP) of Higher Education State Education Ministry, and the Partner-Group of the Chinese Academy of Sciences-the Max Planck Society.

Supporting Information Available: XRD patterns, FESEM images, TG−DTA curves, absorption spectra. This material is available free of charge via the Internet at http://pubs.acs.org.

References

(1) (a) Caruso, F.; Caruso, R. A.; Möhwald, H. *Science* **1998**, *282*, 111. (b) Bergbreiter, D. E. *Angew. Chem., Int. Ed.* **1999**, *38*, 2870. (c) Huang, H.; Remsen, E. E. *J. Am. Chem. Soc.* **1999**, *121*, 3805. (d) Mandal, T. K.; Fleming, M. S.; Walt, D. R. *Chem. Mater.* **2000**, *12*, 3481.

(2) (a) Sun, X.; Li, Y. *Angew. Chem., Int. Ed.* **2004**, *43*, 3827. (b) Dhas, N. A.; Suslick, K. S. *J. Am. Chem. Soc.* **2005**, *127*, 2368. (c) Lu, L.; Capek, R.; Kornowski, A.; Gaponik, N.; Eychmüller, A. *Angew. Chem.Int. Ed.* **2005**, *44*, 5997. (d) Xu, Q.; Tonks, I.; Fuerstman, M. J.; Love, J. C.; Whitesides, G. M. *Nano Lett.* **2004**, *4*, 2509. (e) Jeong, U.; Wang, Y.; Ibisate, M.; Xia, Y. *Adv. Funct. Mater.* **2005**, *15*, 1907. (f) Yang, R.; Li, H.; Qiu, X.; Chen, L. *Chem. Eur. J.* **2006**, *12*, 4083.

(3) (a) Hentze, H. P.; Raghavan, S. R.; McKelvey, C. A.; Kaler, E. W. *Langmuir* **2003**, *19*, 1069. (b) Schmidt, H. T.; Ostafin, A. E. *Adv. Mater.* **2002**, *14*, 532. (c) Landfester, K. *Adv. Mater.* **2001**, *13*, 765. (d) Zu Putlitz, B.; Landfester, K.; Fischer, H.; Antonietti, M. *Adv. Mater.* **2001**, *13*, 500. (e) Gong, Q.; Qian, X.; Ma, X.; Zhu, Z. *Cryst. Growth Des.* **2006**, *6*, 1821. (f) Zhang, D.; Qi, L.; Ma, J.; Cheng, H. *Adv. Mater.* **2002**, *14*, 1499. (g) Ma, Y.; Qi, L.; Ma, J.; Cheng, H. *Langmuir* **2003**, *19*, 4040. (h) Yang, H.; Zeng, H. *Angew. Chem., Int. Ed.* **2004**, *43*, 5206.

(4) (a) Yang, H. G.; Zeng, H. C. *J. Phys. Chem. B* **2004**, *108*, 3492. (b) Liu, B.; Zeng, H. C. *Small* **2005**, *1*, 566–571. (c) Chang, Y.; Teo, J. J.; Zeng, H. C. *Langmuir* **2005**, *21*, 1074. (d) Li, J.; Zeng, H. C. *Angew. Chem., Int. Ed.* **2005**, *44*, 4342.

(5) (a) Yin, Y.; Rioux, R. M.; Erdonmez, C. K.; Hughes, S.; Somorjai, G. A.; Alivisatos, A. P. *Science* **2004**, *304*, 711–714. (b) Liu, B.; Zeng, H. C. *J. Am. Chem. Soc.* **2004**, *126*, 16744.

(6) Lu, C. H.; Qi, L. M.; Yang, J. H.; Wang, X. Y. *Adv. Mater.* **2005**, *17*, 2562.

(7) Cao, H. L.; Qian, X. F.; Wang, C.; Ma, X. D.; Yin, J.; Zhu, Z. K. *J. Am. Chem. Soc.* **2005**, *127*, 16024.

(8) He, T.; Chen, D. R.; Jiao, X. L.; Wang, Y. L. *Adv. Mater.* **2006**, *18*, 1078.

(9) Lu, X. M.; Au, L.; Mclellan, J.; Li, Z. Y.; Marquez, M.; Xia, Y. N. *Nano Lett.* **2007**, *7*, 1764.

(10) Lou, X. W.; Yuan, C. L.; Zhang, Q.; Archer, L. A. *Angew. Chem., Int. Ed.* **2006**, *45*, 3825.

(11) Wang, W. Z.; Poudel, B.; Wang, D. Z.; Ren, Z. F. *Adv. Mater.* **2005**, *17*, 2110.
(12) Gong, Q.; Qian, X. F.; Zhou, P. L.; Yu, X. B.; Du, W. M.; Xu, S. H. *J. Phys. Chem. C* **2007**, *111*, 1935.
(13) Hua, G. Y.; Zeng, H. C. *Angew. Chem., Int. Ed.* **2004**, *43*, 5930.
(14) Dwyer, C. O.; Navas, D.; Lavayen, V.; Benavente, E.; Ana, M. A. S.; González, G.; Newcomb, S. B.; Torres, C. M. S. *Chem. Mater.* **2006**, *18*, 3016.
(15) Piao, Y. Z.; An, K. J.; Kim, J.; Yu, T.; Hyeon, T. *J. Mater. Chem.* **2006**, *16*, 2984.
(16) Xu, M. W.; Kong, L. B.; Zhou, W. J.; Lin, H. L. *J. Phys. Chem. C* **2007**, *111*, 19141.
(17) Zhou, X. F.; Zhang, D. Y.; Zhu, Y.; Shen, Y. Q.; Guo, X. F.; Ding, W. P.; Chen, Y. *J. Phys. Chem. B* **2006**, *110*, 25734.
(18) (a) Heller, A. *Acc. Chem. Res.* **1995**, *28*, 503. (b) Ohtani, B.; Iwai, K.; Nishimoto, S.; Sato, S. *J. Phys. Chem.* **1997**, *101*, 3349. (c) Moriguchi, I.; Hidaka, R.; Yamada, H.; Kudo, T.; Murakami, H.; Nakashima, N. *Adv. Mater.* **2006**, *18*, 69. (d) Wang, C. Y.; Groenzin, H.; Shultz, M. J. *J. Am. Chem. Soc.* **2005**, *127*, 9736.
(19) (a) Wu, J. J.; Yu, C. C. *J. Phys. Chem. B* **2004**, *108*, 3377. (b) Li, X. L.; Peng, Q.; Yi, J. X.; Wang, X.; Li, Y. D. *Chem. Eur. J.* **2006**, *12*, 2383.
(20) (a) Adachi, M.; Murata, Y.; Takao, J.; Jiu, J. T.; Sakamoto, M.; Wang, F. M. *J. Am. Chem. Soc.* **2004**, *126*, 14943. (b) Yoshida, R.; Suzuki, Y.; Yoshikawa, S. *J. Solid State Chem.* **2005**, *178*, 2179.
(21) (a) Macák, J. M.; Tsuchiya, H.; Schmuki, P. *Angew.Chem.Int. Ed.* **2005**, *44*, 2100. (b) Yu, H. G.; Yu, J. G.; Cheng, B.; Liu, S. W. *Nanotechnology* **2007**, *18*, 065604.
(22) (a) Li, Y. Z.; Kunitake, T.; Fujikawa, S. *J. Phys. Chem. B* **2006**, *110*, 13000. (b) Zhong, Z. Y.; Yin, Y. D.; Gates, B.; Xia, Y. N. *Adv. Mater.* **2000**, *12*, 206.
(23) Yang, H. G.; Sun, C. H.; Qiao, S. Z.; Zou, J.; Liu, G.; Smith, S. C.; Cheng, H. M.; Lu, G. Q. *Nature* **2008**, *453*, 638.
(24) Chen, S. C.; Tang, C. Y.; Yu, Z. D. *The important inorganic reactions*, Science and technology of Shanghai publishing company Press: Shanghai, 1994; Chapter 1, pp 866.
(25) (a) Wang, Z.; Heising, J. M.; Clearfield, A. *J. Am. Chem. Soc.* **2003**, *125*, 10375. (b) Subbia, A.; Pyle, D.; Rowland, A.; Huang, J.; Narayanan, R. A.; Thiyagarajan, P.; Zon, J.; Clearfield, A. *J. Am. Chem. Soc.* **2005**, *127*, 10826.
(26) Gong, J. Y.; Yu, S. H.; Qian, H. S.; Luo, L. B.; Liu, X. M. *Chem. Mater.* **2006**, *18*, 2012.

CG8010597